Pergamon

Int. J. Heat Mass Transfer. Vol. 38, No. 13, pp. 2367–2381, 1995

0017-9310/95 $9.50+0.00

0017-9310(94)00370-X

A micro/macro model for fluid flow evolution and microstructure formation in solidification processes

B. Q. LI
Department of Mechanical Engineering, Louisiana State University, Baton Rouge, LA 70803, U.S.A.

and

P. N. ANYALEBECHI
Alcoa Technical Center, Alcoa Center, PA 15069, U.S.A.

(*Received* 21 *August* 1994 *and in final form* 30 *November* 1994)

Abstract—A micro/macro model is developed to represent the evolution of fluid flow, temperature field and microstructure formation in solidification processes. The macro model for fluid flow and heat transfer is established using the finite element method coupled with an Eulerian–Lagrangian formulation, while the micro model for nucleation and grain growth is derived based on the principle of statistical physics. The macro and micro models are coupled through an iterative micro/macro time step scheme. The numerical treatment is given. As an example, the integrated micro/macro model is applied to describe the evolution of fluid flow, temperature and the formation of solidification microstructure during the start-up phase in continuous casting of aluminum alloy. Calculated results compare reasonably well with measurements obtained in a commercial scale ingot for both the temperature distribution and the grain size distribution. The results indicate that the fluid flow and temperature fields change drastically at the initial stage but evolve slowly afterwards, and also the average grain size increases with increasing distance from the ingot surface.

1. INTRODUCTION

Solidification involves the liquid-to-solid transformation, and has been a foundation for many engineering processes. Two typical examples of the commercial processes developed based on the solidification principle are the single crystal growth process in the semiconductor industry for producing high purity crystals, and the continuous casting process in the metals industry for producing ingots as well as near net shape products. Solidification also involves complex physical phenomena, which in general may be classified into two categories: the macro-scale phenomena and micro-scale phenomena [1, 2]. The former includes the fluid flow, heat transfer and mass transfer (as well as electrodynamic phenomena when the electromagnetic field is used to assist the solidification process), which take place at an appreciable scale, while the latter refers to nucleation from liquid phase and grain growth upon the nuclei, which are micro-scale events occurring at a small scale hardly measurable with available devices.

Perhaps because of the great disparity in scales, the macro-scale and micro-scale phenomena have been traditionally studied as separate issues in most published work on solidification. Information on fluid flow and temperature distribution in solidification systems is obtained from process models developed from first principles and/or through experimental measurements. These models have contributed significantly to our fundamental understanding of solidification processing and provided guidelines critical for process development and control. Information on nucleation and grain growth during solidification can not be directly assessed as a result of inadequate instrumentation, but it may be deduced from the metallurgical characteristics of solidified materials measured by various microscopes. The studies of this type have provided physical insight into the events taking place at the micro-scale, which eventually lead to the formation of the final metallurgical microstructure. Recently, modeling work has been done to couple the thermal phenomena and micro-scale phenomena for solidification processes. These models have been developed based on simple heat conduction mechanism, with nucleation and grain growth accounted for using the formulae derived from principles of statistical physics, with empirical parameters for kinetics derived from metallographic measurements. Despite these simplifications, some of the work has met with reasonable success in predicting the temperature distribution and microstructure formation in foundry casting processes [3, 4].

Much of the process modeling work on continuous solidification processes has so far centered around

NOMENCLATURE

$\mathbf{A}(U)$	discretized convection matrix
$\mathbf{B}$	discretized volume expansion matrix
$\mathbf{C}$	discretized continuity matrix
C_p	specific heat
$\mathbf{C}^T$	transpose of discretized continuity matrix
$\mathbf{D}$	discretized thermal convection matrix
$\mathbf{E}$	discretized thermal conduction matrix
H	latent heat
f	solid fraction
F	discretized forcing vector
$F_m(Q)$	global forcing vector
$\vec{g}$	gravity vector
$G(T)$	discretized thermal energy forcing function vector
k	thermal conductivity
k_b	Boltzmann constant
K	empirical constant in grain growth rate expression
$\mathbf{K}$	discretized viscosity matrix
$\mathbf{K}_m(Q)$	global stiffness matrix
$L(t)$	ingot length at time t
L_d	length of the mold
L_d	radius of ingot
$\mathbf{M}$	discretized mass matrix
$\mathbf{M}_m(Q)$	global mass matrix
n	outward normal
$\mathbf{N}$	discretized heat capacity vector
$\mathbf{N}_T$	discretized temperature matrix associated with moving nodes
N	nucleation rate
N_0	nucleation rate constant
N_{max}	total nucleation sites
ΔG	nucleation energy
p	pressure
P	discretized unknown pressure vector
Q	global unknown vector
Q_n	global unknown vector at the nth iteration
Q_{n+1}	global unknown vector at the $(n+1)$th iteration
Q_t	global unknown vector at time step t
$Q_{t+\Delta t}$	global unknown vector at time step $t+\Delta t$
r	r coordinate
$R(t)$	radius of grain size at time t
S	free surface
T	temperature
T	discretized unknown temperature vector
T_{in}	inlet temperature
T_{bot}	bottom block temperature
T_r	reference temperature
T_{water}	cooling water temperature
ΔT_0	center of Gaussian distribution
ΔT_σ	standard derivation of Gaussian distribution
ΔT	undercooling
t	time
$\vec{u}$	velocity vector
U	discretized unknown velocity components
$U_{casting}$	casting speed
U_{in}	inlet velocity
v	grain growth velocity
$\vec{z}$	moving node coordinates
Z	coordinate of the moving surface
Z_j	jth movable node on the moving surface
Y	radius of pouring hole
z	z coordinate
$\hat{z}$	unit vector in z-direction.

Greek symbols

β	volume expansion coefficient
$\delta/\delta t$	time derivative following a moving node
ρ	density
ψ	impingement factor
ω	parameter controlling the movement of internal nodes
v	grain growth velocity.

the steady state or quasi-steady state fluid flow and thermal phenomena. Very little has been done to assess the fundamental behavior of the molten metal flow during the start-up phase, i.e. the period from the start of continuous operation until it reaches the steady state [21]. Even less has been done to develop integrated process models for simultaneously predicting the dynamic development of fluid flow, heat transfer and microstructure formation during continuous solidification processes, which have enjoyed widespread use in manufacturing of metal or semiconductor ingots. These integrated process models should be of great value for both solidification process design and improvement and product quality control.

This paper describes a micro/macro modeling methodology by which the evolution of fluid flow and heat transfer (or other macro-scale quantities) is fully integrated with the dynamic development of microstructure formation in solidification processes. Thus, the micro-scale and macro-scale phenomena, traditionally addressed separately, will be assessed in an integrated fashion. The computational methodology is based on the integration of two models: the macro-scale model for fluid flow and heat transfer which is solved by the finite element method, and the micro-scale model for microstructure formation described by the classical nucleation and grain growth theories. In developing this integrated micro/macro com-

putational algorithm, two novel ideas have been introduced. First, the deforming finite elements are applied to describe the dynamic growth of a whole computational domain over which solidification takes place, and a mixed Eulerian–Lagrangian transformation is used to account for the evolution of the accompanying fluid flow and thermal fields in the growing domain. This treatment should be particularly useful for the study of evolving flow and thermals fields during the starting phase of continuous casting processes, which thus far has received little attention. Secondly, the coupling between the macro-scale model and micro-scale model is practically made possible by introducing a nonlinear iterative micro/macro time step scheme. Without such a scheme, the computation would be prohibitively intensive for this magnitude of computational effort.

The motivation for developing such an integrated process model derives from our effort to address two pressing issues of direct relevance to the quality control and process improvement in continuous solidification processes: the dynamic evolution of fluid flow and heat and mass transfer phenomena during the starting phase and the final microstructure characteristics formed in cast metals. Experience with aluminum casting has shown that many defects, such as hot tearing, hot cracking, surface cracking and corner cracking initiate during the starting phase and eventually wind up in the final products. A knowledge of the evolving fluid flow and thermal behavior is of vital importance in elucidating the mechanisms for the formation of these defects, thereby providing a rational basis for process improvement. On the other hand, a micro-scale model capable of predicting microstructure characteristics, such as the secondary arm spacing and grain size, can be very useful for understanding the fundamentals governing the metallurgical characteristics of the casting products, thereby yielding information critical for quality control.

2. MATHEMATICAL FORMULATION

Let us consider the continuous solidification problem as shown schematically in Fig. 1. The coordinate system is cylindrical with axial symmetry, with the z-axis coincident with the casting direction. Here the problem of interest is the transient transport phenomena during the starting phase of the casting operation. To start, the bottom block is moved up to form a cavity with the mold. The cooling water is switched on. The molten aluminum is then introduced into the cavity through the top pouring hole, or more often through a nozzle, until the cavity is filled. The molten metal begins to cool down and subsequently solidifies along the surface of the cavity. As the bottom block is pulled away at a controlled speed, the solidifying surface is directly exposed to the cooling water, resulting in more metal being solidified. The solidified metal is being withdrawn while the molten metal is continuously supplied from the top. Eventually, the process reaches a quasi-steady state, and by then the fluid flow and temperature profile with respect to the mold no longer changes with time. Prior to that, however, the fluid flow and temperature distribution in the system undergo drastic changes and evolve as the casting process approaches the steady state.

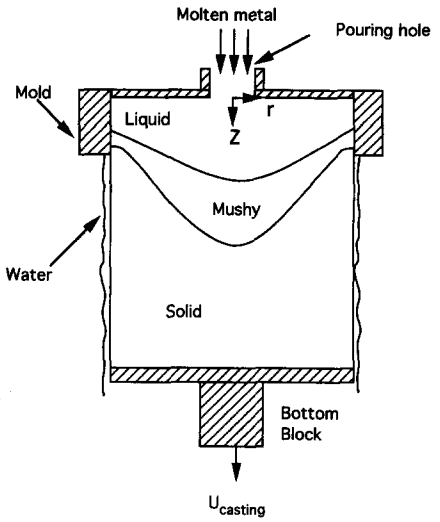

Fig. 1. Schematic representation of dynamic aspects of continuous solidification of aluminum alloys.

While fluid flow and temperature evolve in time at the macro scale, nucleation and grain growth occur at same time but at the micro-scale level, which is undetectable *in situ* using available instruments. These micro-scale events are conceptually represented in Fig. 2 [5]. During solidification, nuclei first form because of thermal fluctuations in the liquid metal that is being cooled below a certain temperature. Some nuclei can not continue to exist because their radius is too small to be stable, while others survive to form a stable cluster. As the temperature continues to decrease, the portion of surviving nuclei increases. These stable nuclei provide the seeding sites onto which liquid molecules can deposit to form crystals or grains. For alloy solidification under consideration, dendritic structure grows after nucleation, followed by coarsening. The remaining liquid finally solidifies at a fixed temperature to form an eutectic structure [1, 2].

2.1. *Formulation of macro-scale phenomena*

The transient fluid flow and thermal development discussed above can be described mathematically by a set of time-dependent nonlinear differential equations: the Navier–Stokes equation for fluid flow and thermal balance equation for temperature distribution along with appropriate boundary conditions.

2.1.1. *Transient fluid flow.* The convective flow in the system described above originates from two sources: one is the momentum of the incoming flow from the nozzle or the pouring hole, and the other from the temperature gradient in the liquid pool. Assuming

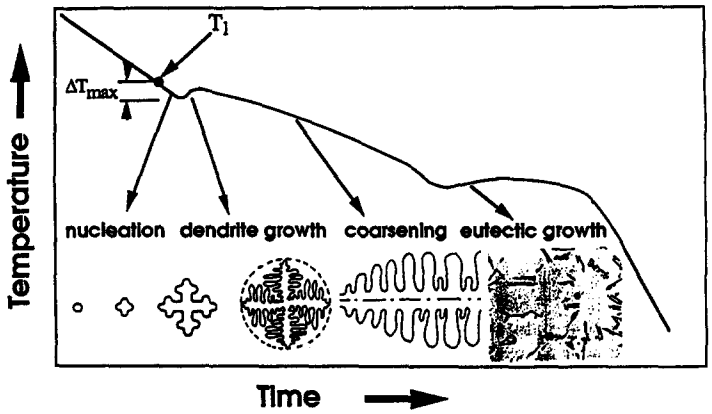

Fig. 2. Formation of microstructure during solidification of metals [5].

that the fluid flow is incompressible and the temperature effect can be approximated in line with Boussinesq's assumption, the transient fluid flow phenomena evolving during the process may be represented by the equation of continuity and the equation of momentum balance [6], namely,

equation of continuity:

$$\nabla \cdot \vec{u} = 0 \tag{1}$$

equation of momentum balance:

$$\rho \frac{\partial \vec{u}}{\partial t} + \rho \vec{u} \cdot \nabla \vec{u} = -\nabla p + \nabla \cdot \mu \nabla T + \rho_r \beta (T - T_r). \tag{2}$$

In the above equations, the subscript r designates a reference state.

2.1.2. *Thermal energy balance.* The transient temperature distribution and hence the solidification process are strongly influenced by the fluid flow field, especially during the starting phase, and are described by the transient thermal balance equation [6]. Neglecting the viscous dissipation, which is a rather small fraction of heat generation, the conservation of thermal energy in the process can be expressed in terms of temperature in the form

$$\rho C_p \frac{\partial T}{\partial t} + \rho C_p \vec{u} \cdot \nabla T = \nabla \cdot k \nabla T + \rho H \frac{df}{dt} \tag{3}$$

where the last term represents the heat contribution released from solidification. In micro/macro modeling, this term serves as a window through which the micro models for solidification are linked to the fluid and thermal calculations. In the above equations, the thermal and physical properties are mixture properties of liquid and solid and are calculated based on the solid and liquid fractions.

2.1.3. *Boundary conditions.* To obtain information on the transient fluid flow and heat transfer phenomena, the above equations must be solved subject to the physical constraints specific to the system or the boundary conditions. In the present study, the no-slip condition is enforced along the solid and liquid interface for the fluid flow calculations. Thermal boundaries are of the Newton cooling type where the heat transfer coefficient in general is temperature dependent. The coefficient can be a strong function of temperature when the effect of both film and boiling heat transfer is considered along the side interface between the solidifying surface and the cooling water [7]. What differentiates this study from other similar studies is perhaps the boundary condition describing the growth of the ingot length as the casting operation proceeds from the beginning. This condition is obtained from the overall mass balance. The inlet flow and thermal conditions are prescribed in accordance with casting conditions. With reference to Fig. 1, the boundary conditions needed for the present numerical study can be mathematically stated as below:

(i) at the bottom of the ingot

$$\frac{dn}{dt} = \vec{u} \cdot n = U_{casting}$$

$$\text{and} \quad -kn \cdot \nabla T = h(T - T_{bot}) \quad \text{at} \quad z = L(t) \tag{4}$$

(ii) on the top of the liquid pool

$$T = T_{in} \quad \text{and} \quad \vec{u} = U_{in}(r)$$

$$\text{at} \quad z = 0 \quad \text{and} \quad r \leqslant Y \tag{5}$$

$$n \cdot \nabla T = 0 \quad \text{and} \quad \vec{u} = 0$$

$$\text{at} \quad z = 0 \quad \text{and} \quad r > Y; \tag{6}$$

(iii) along the side of the liquid pool and the solidifying ingot

$$\vec{u} = 0 \quad \text{and} \quad -kn \cdot \nabla T = h(T - T_{mold})$$

$$\text{at} \quad z \leqslant L_d \quad \text{and} \quad r = L_r \tag{7}$$

$$\vec{u} = (U_{casting}, 0) \quad \text{and} \quad -kn \cdot \nabla T = h(T - T_{water})$$

$$\text{at} \quad z > L_d \quad \text{and} \quad r = L_r. \tag{8}$$

2.2. *Formulation of micro-scale phenomena*

From the principles of statistical physics, nucleation is a fluctuating phenomenon that comes from thermal fluctuations in a liquid. At any moment, the number

of nuclei in the liquid obeys the Boltzmann distribution [1, 8], and may be written as below:

$$N = N_0 \exp\left(-\frac{\Delta G}{k_b T}\right). \quad (9)$$

Although very simple in form, equation (9) poses a problem for computation as the exponential term often leads to an erroneous estimate. To overcome this difficulty, Rappaz [3] proposed that the number of nuclei formed during solidification may be approximated by a Gaussian distribution,

$$\frac{dN}{d(\Delta T)} = \frac{N_{max}}{\sqrt{2\pi}\Delta T_\sigma} \exp\left(-\frac{(\Delta T - \Delta T_\sigma)^2}{2(\Delta T_\sigma)^2}\right). \quad (10)$$

In the case of aluminum casting, grain refiner is added to induce heterogeneous nucleation. Zou and Rappaz [9] showed that equation (10) is still valid provided that N_{max} is treated as the total density of heterogeneous nucleation sites or grain refining particle density added to the liquid aluminum.

There are many models for grain growth on a nucleus. For a grain refined aluminum melt, the grain growth may be described by the following expression [5]:

$$v = \left(\frac{\Delta T}{K}\right)^2 \quad (11)$$

where K is an empirical constant that can be obtained by fitting the measured cooling curves and final grain sizes. When the grain growth velocity is known, the solid fraction may be calculated as,

$$\frac{\partial f}{\partial t} = 4\pi N(t) R^2(t) v(t) \psi \quad (12)$$

with ψ being the factor accounting for grain impingement and $N(t)$ calculated from equation (11). Equations (11) and (12) were used in modeling grain refined aluminum alloy solidification and satisfactory results were obtained [5]. The present study makes use of the above grain growth model with the same empirical constants K and ψ as reported in ref. [5].

3. NUMERICAL TREATMENT

This section discusses the numerical algorithm for the solution of the coupled fluid flow and thermal problem over a time dependent computational domain, as stated by equations (1)–(8). In light of the boundary conditions stated at $z = L(t)$ (equation (4)), the deforming finite elements may be used to model the dynamic growth of the domain over which the fluid flow and thermal phenomena are evolving. For this purpose, the method based on the tracking of the moving computational front using deforming elements is used [10, 11]. When coupled with an automatic time-step control integrator [12], the deforming finite element method provides a powerful means for tackling time dependent free surface problems. In view of the relatively simple geometry of the moving front ($z = L(t)$) under consideration, it is conceivable that this transient algorithm may be modified with minimal effort to model our time-dependent fluid flow and thermal problems. As the numerical algorithm for the deforming elements has been detailed elsewhere [11], only a brief account of the procedure, as modified for the present study, is given below.

It is remarked here that there exists an internal moving front defined by the heat flux jump at the eutectic point. From the heat transfer point of view, solidification of eutectic liquid occurs at a fixed temperature or the eutectic temperature in much the same way as a pure liquid solidifies at the melting point. This has been detailed by Flemings [2] with a reference to phase diagram. Thus, the eutectic solidification can be treated numerically in the same fashion as used for pure liquid solidification. Both fixed and moving grid algorithms have been developed for the purpose of numerical simulation of pure liquid solidification. The fixed grid approach, or more specifically the enthalpy approach [13], is often used for alloy solidification which ends at the eutectic point and is adopted for the present study.

The discussion of the numerical treatment is facilitated by starting from the finite element solution of fluid flow and thermal problems over a fixed domain. The finite element solution procedure is now well established and details are documented in many textbooks on the finite element analysis of continuum mechanics problems [14, 15]. Following the standard Galerkin finite element procedures, one obtains the following finite element form of solutions for the fluid flow and temperature field equations:

$$\mathbf{C}^T U = 0 \quad (13)$$

$$\mathbf{M}\frac{dU}{dt} + \mathbf{A}(U)U + \mathbf{K}U - \mathbf{C}P + \mathbf{B}T = F \quad (14)$$

$$\mathbf{N}\frac{dT}{dt} + \mathbf{D}(U)T + \mathbf{E}T = G(T) \quad (15)$$

where the boldfaced letters are system matrices. Note that F and G are the forcing functions for the system which include volume forces, latent heat and boundary conditions.

The application of the deforming finite element method to solve the coupled fluid flow and thermal problem under consideration entails modifying the above equations by incorporating the effect of the computational domain expansion caused by the moving boundary. To facilitate the discussion, the kinematic boundary condition at the moving front $z = L(t)$ is rewritten as follows:

$$\frac{dS}{dt} = \frac{\partial S}{\partial t} + \bar{u} \cdot \nabla S = 0 \quad (16)$$

where $S(L, t) = 0$ defines the free surface. This equation is more a general statement than equations (4). It represents a Lagrangian description of the free surface

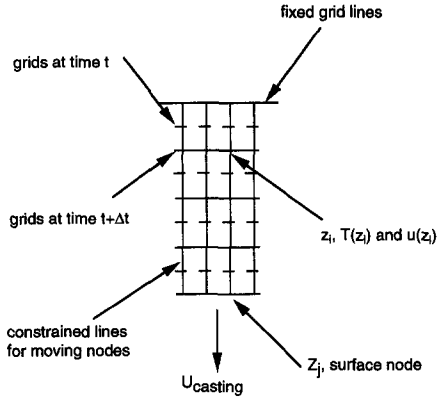

Fig. 3. Movement of free boundary nodes and internal nodes in transient calculations.

boundary, that is, the particles on a moving surface always remain stationary with respect to the surface [16].

The concept of keeping track of the moving surface is to allow the points defining the surface to move and to solve their moving coordinates as part of the total unknowns. To prevent over-distortion of the elements associated with the moving front, some internal nodes are also allowed to move accordingly but in a controlled fashion. The basic idea is illustrated in Fig. 3. The internal nodes are moved in relation to the moving surface nodes in the following manner [10, 11],

$$z_i = \omega_i Z_j. \tag{17}$$

Thus, the ith internal node ($z_i = z_i(Z_j, t)$) deforms in accordance with the movement of Z_j, with ω_i the parameter determining the relative distance between the ith internal node and the ith corresponding moving boundary node.

Equations (1)–(11) are derived with reference to the Eulerian frame in which the space coordinates are fixed. They need to be transformed to the coordinates defined by the moving nodes. This can be done using the mixed Eulerian–Lagrangian formulation. According to this formulation, the Eulerian time derivative is related to the Lagrangian time derivative, which is taken in the frame floating with the moving nodes along the constrained lines, in the following manner [10, 11],

$$\frac{\delta}{\delta t} = \frac{\partial}{\partial t} + \frac{\delta \vec{z}}{\delta t}\cdot\nabla = \frac{\partial}{\partial t} + \frac{\delta Z}{\delta t}\frac{\partial \vec{z}}{\partial Z}\cdot\nabla. \tag{18}$$

With this transformation rule, the Eulerian time derivatives can be converted to those defined on the moving nodes and the finite element discretization can then be applied to solve the problem. If equation (18) is applied to the temperature field T, one has

$$\frac{\partial T}{\partial t} = \frac{\delta T}{\delta t} - \frac{\delta Z}{\delta t}\frac{\partial \vec{z}}{\partial Z}\cdot\nabla T. \tag{19}$$

Similar transformations can be applied to the velocity field and the moving front equation stated by equation (16). Equation (19) and the similar velocity and moving boundary equations can be cast in the finite element form using the Galerkin method. For instance, the following discretized equation can be obtained for the temperature field,

$$\mathbf{N}\frac{\mathrm{d}T}{\mathrm{d}t} = \mathbf{N}\frac{\delta T}{\delta t} - \mathbf{N}_T\frac{\delta Z}{\delta t}. \tag{20}$$

With these ingredients, the final equation for our problem can be obtained. Upon substituting equation (20) and the like into equations (13)–(15), combining the resultant equations with the discretized form of the kinematic boundary condition, and rearranging, one obtains a system of time dependent ordinary differential equations as below.

$$\mathbf{M}_m(Q)\frac{\delta Q}{\delta t} + \mathbf{K}_m(Q)Q = F_m(Q) \tag{21}$$

where the matrices of mass and diffusion/convection, $\mathbf{M}_m$ and $\mathbf{K}_m$, the unknown vector Q and force vector F_m take the following forms,

$$\mathbf{M}_m(Q) = \begin{bmatrix} \mathbf{M}(X) & 0 & 0 & -\mathbf{M}_U(U,X) \\ 0 & 0 & 0 & 0 \\ 0 & 0 & \mathbf{N}(X) & -\mathbf{N}_T(T,X) \\ 0 & 0 & 0 & \mathbf{M}_f(X) \end{bmatrix} \tag{22}$$

$$\mathbf{K}_m(Q) = \begin{bmatrix} \mathbf{K}(X)+\mathbf{A}(U,X) & -\mathbf{C}(X) & \mathbf{B}(X) & 0 \\ -\mathbf{C}^T(X) & 0 & 0 & 0 \\ 0 & 0 & \mathbf{D}(U,X)+\mathbf{E}(X) & 0 \\ \mathbf{K}_n(X) & 0 & 0 & 0 \end{bmatrix} \tag{23}$$

$$Q = \begin{bmatrix} U \\ P \\ T \\ X \end{bmatrix} \quad F_m(Q) = \begin{bmatrix} F(X) \\ 0 \\ G(T,X) \\ 0 \end{bmatrix}. \tag{24}$$

Equation (21) can be solved using any time-integration scheme. If the backward implicit time integration is used, it is approximated by

$$(\mathbf{M}_m + \mathbf{K}_m\Delta t)Q_{t+\Delta t} = F_m\Delta t + M_m Q_t. \tag{25}$$

The above equation is a nonlinear because $\mathbf{M}_m$, $\mathbf{K}_m$ and F are all a function of $Q_{t+\Delta t}$. It can be efficiently solved by employing the Newton–Raphson method. The unknowns can now be calculated. The calculation starts with a given initial condition and a given time step. Equation (26) is solved iteratively and converged results for the time step are then used as initial values to the next time step. This way, the calculation continues on in time until a steady state is reached or the preset time ending criterion is met.

4. SOLIDIFICATION MODELING

Two aspects associated with alloy solidification modeling are the drastic change in liquid viscosity and the release of latent heat due to phase transformation. The former affects the fluid flow behavior while the latter the temperature distribution. There exist two main approaches to account for the effect of solidification on the liquid flow, both of which are empirical. One is to simulate the mushy zone and solidification effect by introducing a drag function [17] and the other by treating the viscosity of the alloy as a function of temperature [18]. The latter is used in this study as it may also help stabilize the numerical calculations by the finite element method. The temperature dependency of viscosity used in obtaining the results presented below takes the exponential form determined experimentally by Joly and Mehrabian [19].

In alloy solidification processes, the latent heat release is closely related to the solid fraction evolution. There are many documented models for calculating solid fraction during solidification. For the coupled micro/macro model presented in this study, the solid fraction evolution during solidification is directly evaluated by equation (12), which along with equation (10) is applied to predict the grain structure during solidification. These equations may be readily discretized and incorporated into the above fluid flow and heat transfer calculations.

5. COUPLING BETWEEN MICRO-MODEL AND MACRO-MODEL

Mathematically, the coupling between the micro model and macro model requires the simultaneous solution of equations (3) and (12). The temperature predicted from the macro model is used to calculate the nucleation rate, grain size and solid fraction evolved during solidification. The solid fraction so estimated is then fed back to the momentum and thermal balance equations for updating the temperature distribution. As the time scales are significantly different for nucleation and fluid flow variation, an appropriate time step must be carefully chosen to make the numerical computation possible. If a micro time step, say, 1×10^{-6} s or smaller, is chosen in order to represent the nucleation phenomenon, then a computation of fluid flow and thermal field for a time period of 15 min would require 9×10^8 time steps. Assuming one converged nonlinear iteration needs a CPU time of 3 min (which is typical on an SGI used for our calculations), a total of 2.7×10^9 CPU min or about 5200 years would be required, an almost astronomical number that no one could afford! To overcome this difficulty, we devised the following iterative micro/macro time step scheme, which is then integrated with the conventional implicit time matching algorithm for thermal and flow calculations [14].

First, an appropriate time step is chosen based purely on the fluid flow and temperature calculations. The selection of the time step may be based on the error estimate, which can be made automatic using the available strategies [12]. The temperature distribution calculated at the node points this way is then used in calculations for microstructure formation. To do so, it is assumed that over a micro time step for microstructure calculation, the fluid flow velocity, temperature distribution and node coordinates are each interpolated as a linear function of time. The solid fraction evolved during solidification is accumulated and is then fed back to re-calculate the temperature and fluid flow field. This micro- and macro-time iteration then continues for one macro time step until the calculated unknowns for both macro-scale and micro-scale parameters meet the preset convergence criteria. A new macro time step is then selected and another set of micro and macro time step iterations is made. The calculation proceeds in this fashion until the total time period preset for the simulation is reached. This macro and micro coupling scheme is schematically represented in Fig. 4.

6. SOLUTION METHOD

The above equation is solved by modifying the general purpose finite element program for fluid flow, FIDAP. The modifications include incorporating the micro model for solidification, the iterative micro/macro time step scheme, the temperature dependent heat transfer coefficients and the temperature dependent viscosity. The free surface feature of the program is exploited to perform the simulation of the dynamic growth of the ingot during solidification. The results presented below were obtained from the micro/macro model along with the automatic time step control scheme as suggested by Gresho *et al.* [12]. The calculations used 1488 four-node elements with only a portion of the nodes (1100 nodes) being allowed to move. A typical calculation for the evolving fluid flow and temperature fields and microstructure formation required about 18–34 CPU h on a single processor Silicon Graphics workstation (Model-380).

7. COMPUTED RESULTS AND DISCUSSION

The finite element-based integrated micro/macro model presented above permits the prediction of the evolution of the fluid flow field, the temperature field and the formation of solidification microstructure in a solidifying ingot from start-up to steady state during continuous casting operations. Numerical computations start with the filling of the molten metal in the cavity, which is formed by lifting the bottom block to level with the water cooled mold. Because of limited space, only a selection of the computed results will be presented below. The results are for a round ingot with a diameter of 0.40 m and for a casting speed of 9.0×10^{-4} m s^{-1}. The condition of axial symmetry was assumed. The physical and thermal property data for the calculations were taken from ref. [13].

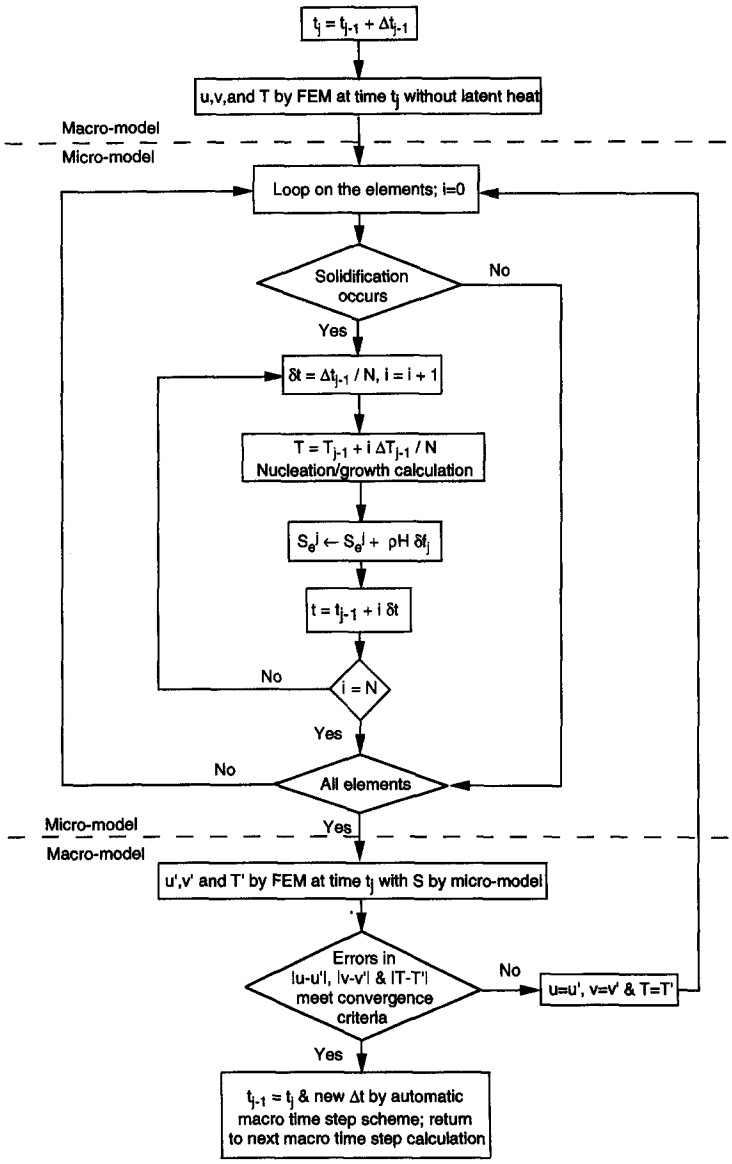

Fig. 4. The iterative micro/macro time step scheme for coupling between the macro-scale model and the micro-scale model.

7.1. *Evolution of fluid flow and temperature distribution*

In simulating the start-up phase of a continuous casting process, both the growing of solidifying ingot length and the transient thermal and flow fields evolving in the ingot must be resolved simultaneously. Figure 5 shows the evolution of the ingot length from the beginning of casting up to a steady state, while Figs. 6–9 depict the unfolding vector velocity field, streamline profiles, temperature field and liquid–solid transformation as the casting operation proceeds. The pictures shown are oriented such that the casting direction is in the z-direction and the axis of symmetry coincides with the left-hand side of the picture. In this set of calculations, only a portion of the internal nodes has been allowed to move in accordance with the moving boundary. These figures clearly demonstrate that the large deformation caused by the growth of the ingot and the accompanying transient fluid flow, thermal and solidification phenomena in the round ingot casting process can be very well simulated by the deforming finite element method described earlier.

Examination of the set of pictures in Figs. 6–8 reveals the general trend of the dynamic fluid flow and thermal development within the growing, solidifying ingot: there are drastic changes in fluid flow and temperature initially but these changes proceed more slowly as the process approaches a steady state. The flow in the liquid pool is predominantly driven by the temperature gradient and the flow from the inlet has an almost negligible effect on the flow field. Figures 6 and 7 show that the recirculation loop grows quickly initially, but it becomes relatively stable after about

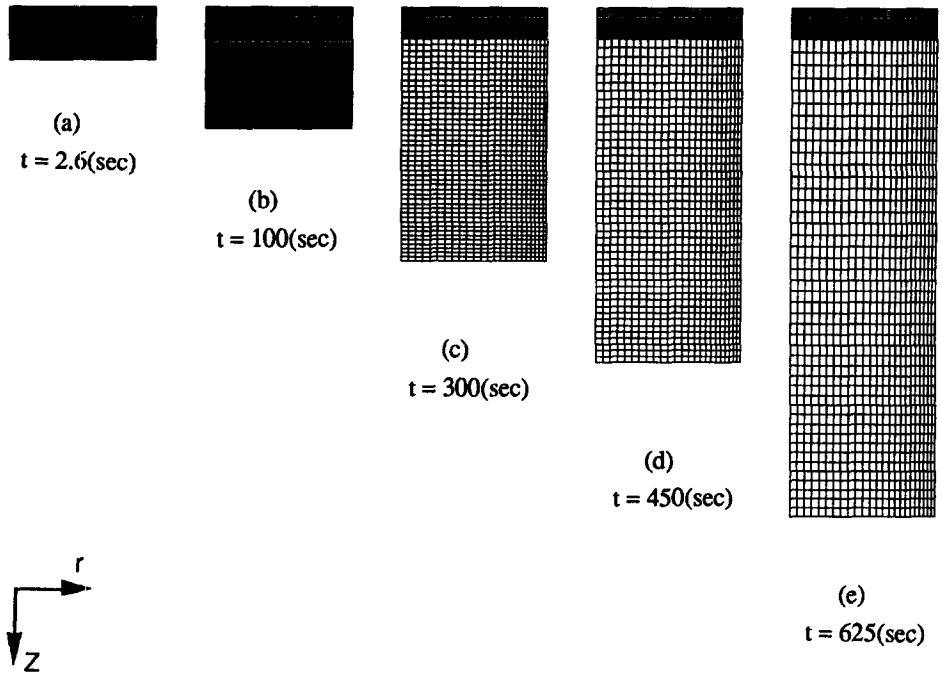

Fig. 5. Expansion of finite element grids to simulate the growth of the ingot length during the starting phase of the round ingot casting process.

100 s. The corresponding evolution of the thermal field follows the same fashion in that the temperature field changes quickly at the start of the operation and the changes slow down afterwards, as illustrated in Fig. 8. This dynamic behavior of fluid flow and thermal fields is as expected from first principles and is in general agreement with casting experience [20]. Figure 6(a) shows the fluid flow field at $t = 2.6$ s after the casting has started. From the corresponding temperature field (Fig. 8(a)), it is evident that cooling first starts along the water cooled mold and the bottom block. At the subsequent stage, more molten metal is poured in from the top, and consequently the thermal energy in the system increases. At the same time more heat is

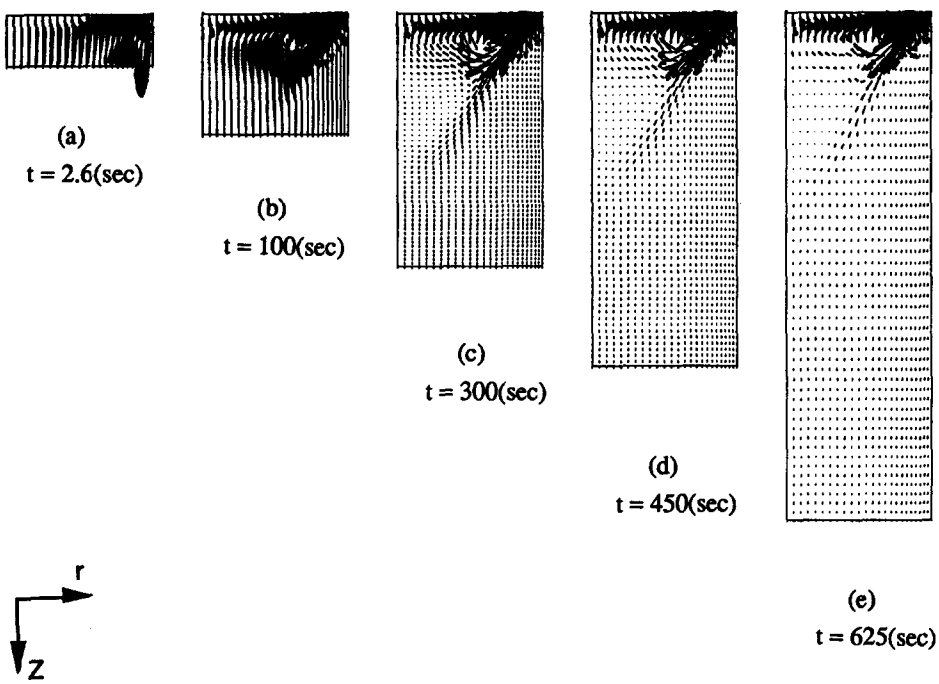

Fig. 6. Transient development of the fluid flow field in the growing round ingot during the starting phase. The molten metal inlet velocity is 3.6×10^{-3} m s^{-1}.

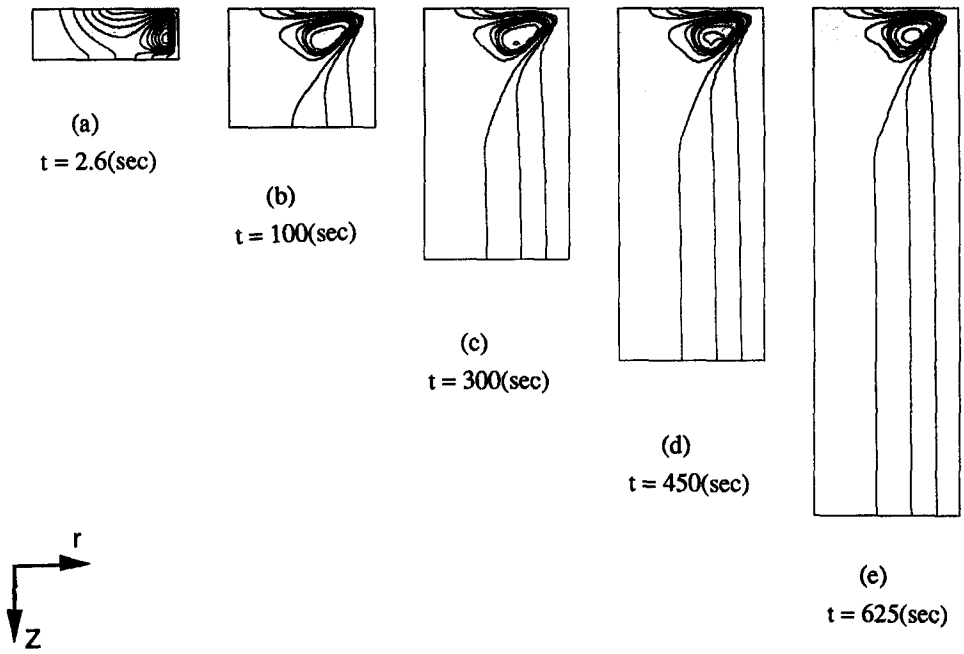

Fig. 7. The corresponding stream line profiles of the velocity field shown in Fig. 6.

removed from the system as the downward movement of the bottom block exposes more solidifying surface to the cooling water. Since heat is extracted at a slower pace than input from the molten metal, thermal energy builds up in the system, which is evidenced by the larger area of higher temperature (Fig. 8(b)). The ensuing temperature field evolves in the same manner but less drastically as the process continues until a steady state is reached and the thermal energy brought in by the incoming metal is balanced by what is extracted from the system. From the last three sets of plots in Figs. 5–7, it is apparent that the fluid flow field in the liquid pool and the isothermal contours in the region around the mold become almost stationary with respect to the top surface. This suggests that a quasi-thermal-equilibrium has been established. However, in the region below the mold and especially near the bottom, the temperature profiles are still develop-

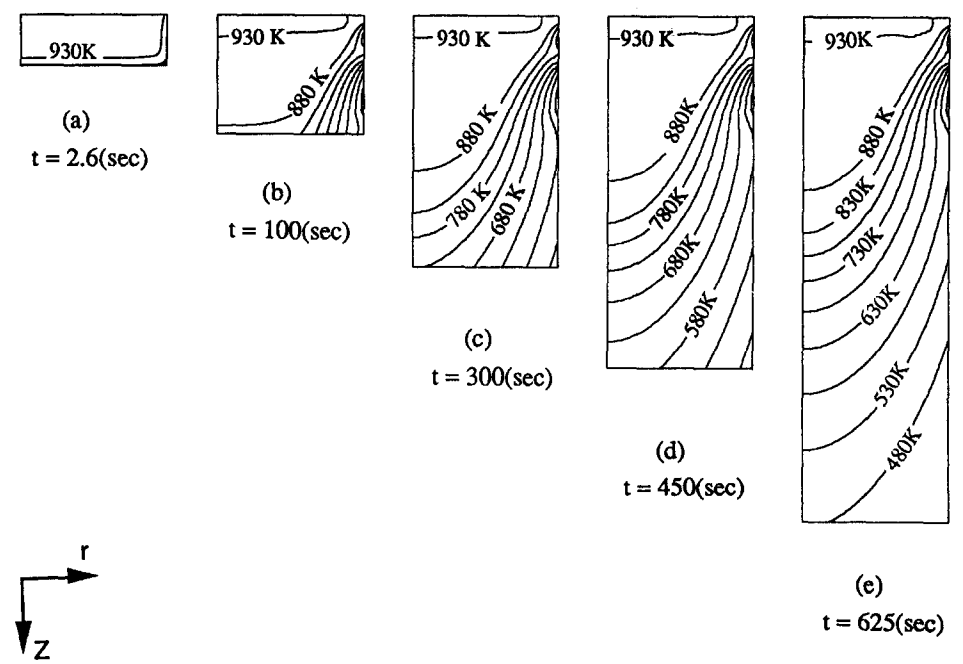

Fig. 8. Evolution of temperature distributions in the growing round ingot during the starting phase.

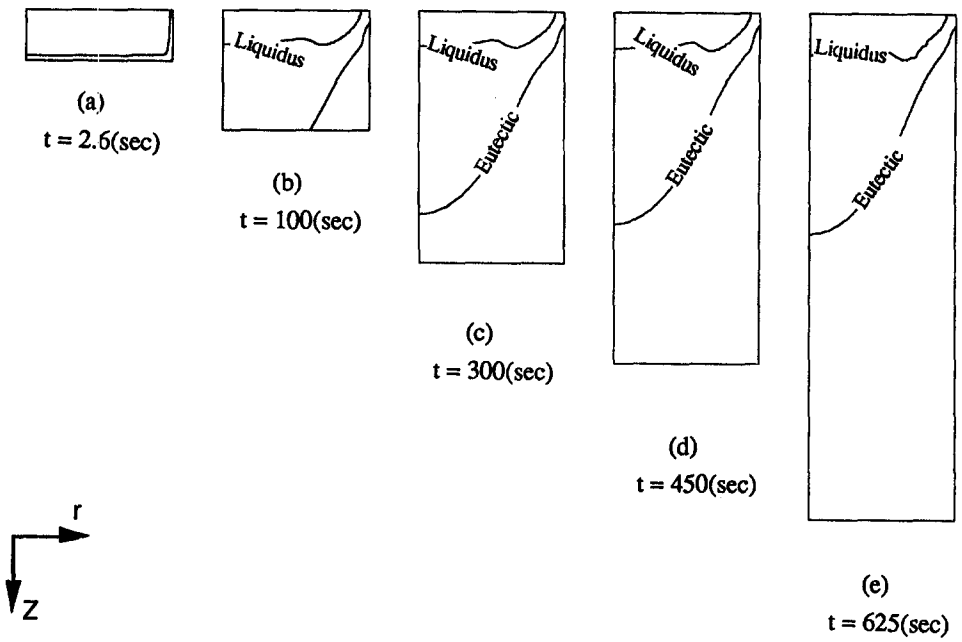

Fig. 9. Evolution of mushy zone region in the growing round ingot during the starting phase.

ing but again much more slowly than at the initial stage. From Fig. 8(e) as well as those calculated for longer times, it is found that a great portion of the ingot reaches the quasi-steady state except near the bottom block. Thus, it may be reasonable to argue that Fig. 8(e) represents approximately the quasi-steady state. The corresponding dynamic solidification behavior in the system also deserves a note. As shown in Fig. 9, the mushy zone region quickly expands initially (Figs. 9(a) and (b)), but the expansion slows down afterwards. It eventually reaches the quasi-steady state after which the mushy zone size no longer changes, as evident in Fig. 9(e).

To verify the results computed from the micro/macro model, a set of thermal measurements under a steady state condition were made in a commercial-scale ingot. The techniques used in the measurements are similar to those stated elsewhere [21]. Figure 10 shows the comparison of the calculated and measured results for the temperature distribution along the center line of the ingot under the steady state condition. It is clear that the prediction is in reasonably good agreement with the measurement. Note also that the steep decrease in temperature after the solidification is completed is also very well predicted by the micro/macro model.

7.2. *Solidification microstructure*

The solidification microstructure of the ingot is shown in Fig. 11. The polarized light photomicrographs illustrate that the microstructure is characterized primarily by equiaxed grains, with some duplex structure (a mixture of fine dendrites and coarser cellular dendrites) occurring some distance away from the surface towards the center of the ingot. The grain size becomes larger as the distance from the ingot surface increases. This is consistent with the conclusions made based on the theory of solidification processing [1, 2], and can be explained by the change in the local solidification rate, that is, the distance between the solidus and liquidus divided by the time a particle travels from the solidus to the liquidus. In view of the macro-scale results for the thermal and mushy zone contours as shown in Figs. 8 and 9, the local solidification rate decreases with increasing distance from the ingot surface. As the ingot surface is directly exposed to the cooling water, a larger temperature gradient exists near the surface (see also Fig. 8) and hence a higher solidification rate there. This high solidification rate gives a fine grained microstructure, as shown in the upper picture in Fig. 11. The radial heat transfer away from the surface inward is by heat conduction, resulting in a smaller temperature gradient and hence a lower solidification rate. This gives rise to somewhat bigger grain size, as illustrated in the middle metallograph in Fig. 11. The largest gap between the liquidus and solidus lines along the center line is clearly a manifestation of the lowest solidification rate, and therefore the largest grain size, as appears in the lower photograph in Fig. 11.

As mentioned earlier, one of the distinct features of the micro/macro model developed in this study is that the model is capable of predicting the microstructure characteristics for ingots with equiaxed grain structures. Such grain structures often occur in aluminum alloys with additions of grain refiners, as shown in Fig. 11. The grain size of the ingot can be determined by metallographic measurements, and the results for average grain size, along with the standard variation,

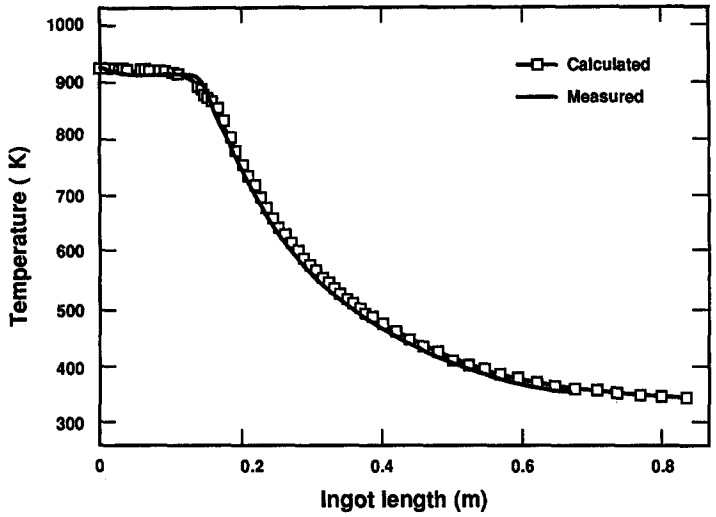

Fig. 10. Comparison of computed and measured results for centerline axial temperature distribution under a steady state condition during continuous casting of aluminum alloys.

are shown in Fig. 12 as a function of the distance from the ingot surface. To compare with the measured results, the grain size distribution predicted by the micro/macro model as a function of radius is also plotted in Fig. 12. Inspection of Fig. 12 indicates that the calculated grain size distribution agrees with the measured one within the error margins associated with the measurements. Both the predicted and measured results show that the average grain size increases inward from the ingot surface. It is noteworthy that slightly finer grains are predicted by the micro/macro model while a larger grain size is calculated at the center.

7.3. *Discussion*

There are several important aspects associated with the present micro/macro model that merit discussion. First, the micro/macro model appears to be the first integrated process model addressing simultaneously the growth of the ingot, macroscopic fluid flow and heat transfer for process design and optimization and solidification microstructure for quality control. While the model is specifically developed for continuous casting of aluminum alloys, the modeling methodology is general in that it should be readily applied to other casting processes, such as investment casting, die casting and mold casting. Indeed, if appropriate boundary conditions are imposed and casting velocity is set to zero, the model can be directly used to predict the same macro- and micro-scale phenomena in solidification of equiaxed grain structures in other solidification processes. Moreover, if an appropriate micro kinetic model can be derived for the formation of other solidification structures, a similar micro/macro model can be developed by using the same micro/macro coupling scheme.

It should be pointed out that a micro/macro coupling scheme has also been proposed by Rappaz and co-workers [3, 9], but it differs from the present micro/macro time step coupling algorithm in several aspects. First of all, his scheme has no automatic time step control. While it may be sufficient for simplified solidification systems for a demonstration purpose, it is doubtful that the scheme has an adequate efficiency for more complicated computations. Also, the scheme is linear and it is difficult to be extended to nonlinear fluid flow calculations. Most important of all, according to his scheme the temperature distribution is predicted using the solid fraction calculated from the temperature field at the previous macro time step.

Clearly, significant errors may result unless the macro time step is small enough. These errors may propagate and accumulate as the time matching calculation continues, thereby having a potential for resulting in incorrect predictions. It should be stressed here that the errors in the estimation of solid fraction still can not be corrected even if an automatic time step control strategy would be applied.

In solidification processing of materials, thermal stresses arising due to solidification are often the origin of casting defects, such as hot cracking and hot tearing. In calculating the thermal stresses, information on the history of the temperature distribution and of the particle path in the ingot is needed. The above computational methodology provides a useful means by which the needed thermal information can be calculated and can be readily linked to a thermal stress model, thereby facilitating the development of a combined thermoflow and thermostress model for solidification processes. The frequently used mathematical models, developed based on the steady state solidification theory, would not provide the needed information on the evolution of temperature distribution and particle history, and thus would be difficult to integrate directly with thermal stress models.

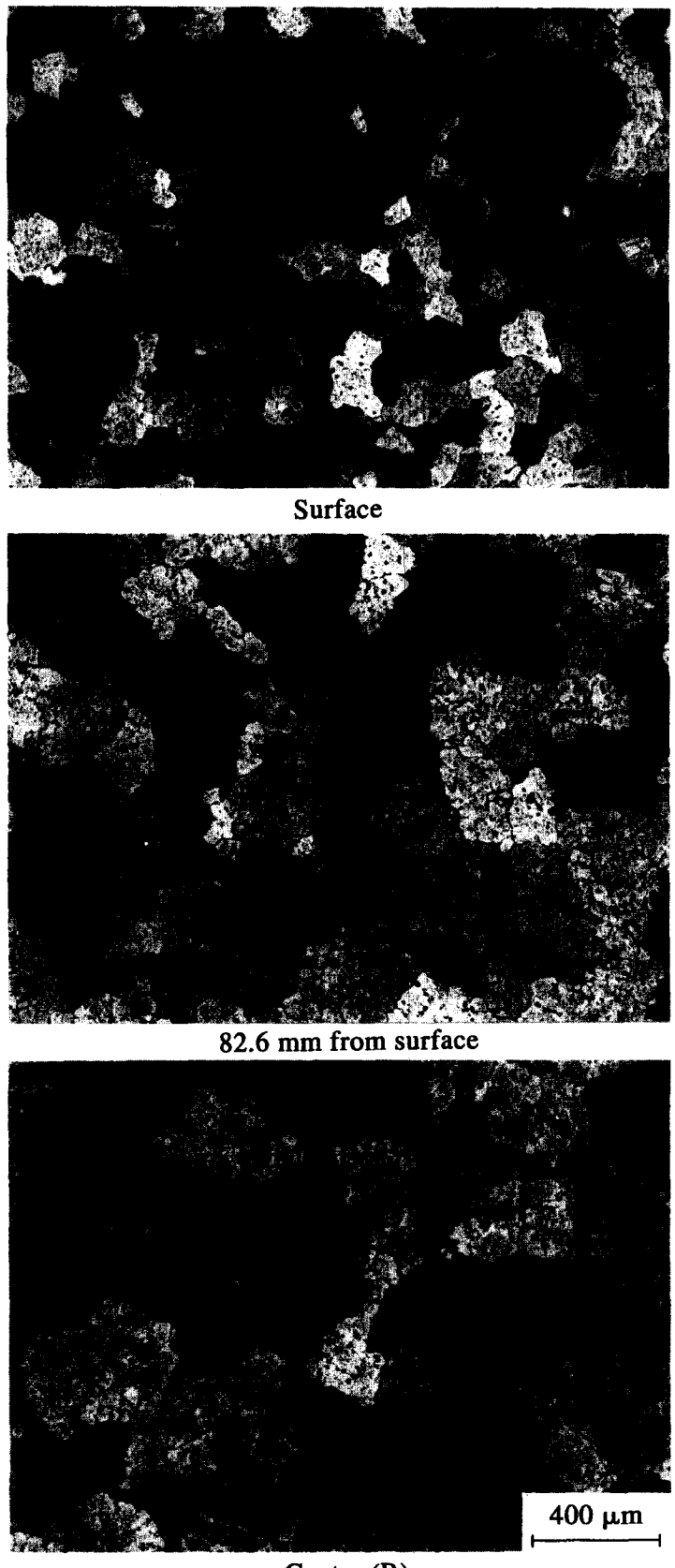

Fig. 11. Polarized light microphotographs showing the grain morphology and size as a function of distance from ingot surface.

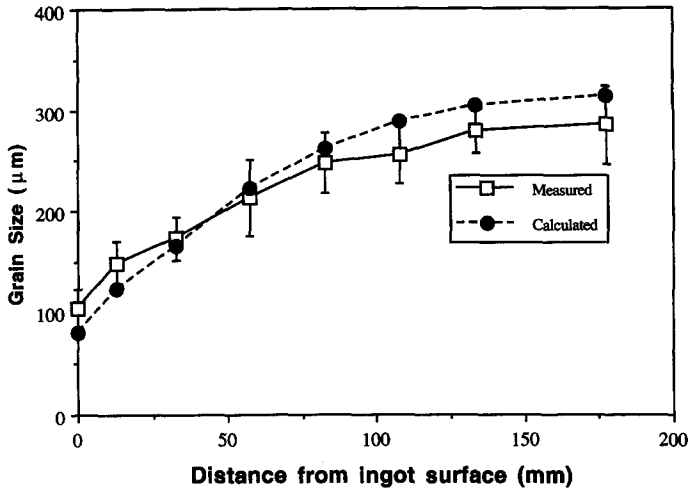

Fig. 12. Comparison of calculated and measured average grain size distribution as a function of radial distance from ingot surface in the continuously cast ingot.

While the micro/macro time step scheme described above is very useful for simultaneously predicting fluid flow, temperature distribution and microstructure formation during solidification, it is considered computationally intensive and thus should be dispensed with when the microstructure is not a predicted parameter. If, for example, only the thermal and flow fields are of the main concern [20, 22], as in the case of thermal stress calculations, the micro model can be replaced by much simpler and computationally more economical models, such as the Scheil model, for solid fraction evolution. Our numerical experiments showed that the solid fraction and temperature profiles predicted by the micro model (with nucleation and grain growth) and the Scheil model [2] are almost the same, except that the use of the micro model has an advantage of yielding information on grain size distribution. As the only variable in the Scheil model is temperature, no iterative micro/macro coupling scheme is needed, thereby resulting in substantial savings in computing time [20, 22] if only the macro variables such as melt flow velocity and temperature distribution are sought for.

Finally, it is noteworthy that the above calculations are formulated and illustrated for axially symmetric conditions. However, the algorithm should be more general, and directly applicable to two- or three-dimensional calculations. Of course, considerably more memory space, disk storage and also CPU time would be required for a three-dimensional calculation.

8. CONCLUDING REMARKS

This paper has presented a micro/macro model for the transient evolution of fluid flow, heat transfer and microstructure formation during solidification processes. The macro model describes the dynamic development of fluid flow and temperature distribution and is developed based on the deforming finite element concept, combined with an Eulerian–Lagrangian formulation, while the micro model represents the nucleation and grain growth during solidification. The continuous casting of aluminum has been used as an example. The expansion of the solidifying ingot during the starting phase has been modeled as a special case of general free moving boundary problems, with the moving boundary nodes solved as part of the total unknowns. The coupling of the macro and micro models has been made possible by an iterative micro/macro time step scheme, by which the macro scale variables are assumed to vary linearly over an iterative micro time step for computation of nucleation and grain growth phenomena. The effect of solidification on the fluid behavior has been modeled by the temperature dependent viscosity and the latent heat release by the micro model. Numerical results for continuous solidification of a round ingot have been presented, and good agreement is obtained between the computed results and experimental measurements for temperature distribution in the caster. The results showed that the fluid flow and temperature distribution change rapidly at the initial stage but the change slows down later in the process. The microstructure of the cast metal is characterized by equiaxed grain structure. The average grain size distribution predicted by the micro/macro model agreed reasonably well with the measured results. Both measured and computed results showed that the average grain size decreases with distance from the ingot surface, which is as expected from the theory of solidification processing.

Acknowledgements—The work was supported in part by Alcoa's Transport and Solidification Process Design Science Program. The authors are grateful for helpful comments and discussions from Dr D. P. Ziegler at Alcoa Technical Center, Alcoa Center, PA, U.S.A.

REFERENCES

1. W. Kurz and D. J. Fisher, *Fundamentals of Solidification*, Trans. Tech. Pub., Aedermannsdorf, Switzerland (1986).
2. M. C. Flemings, *Solidification Processing*, Chap. 5. McGraw-Hill, New York (1974).
3. M. Rappaz, Modeling of microstructure formation in solidification processes, *Int. Mater. Rev.* **34** (3), 93–123 (1989).
4. M. Rappaz and D. M. Stefanescu, Modeling of microstructure evolution. In *Metals Handbook* (9th Edn), Vol. 15, pp. 883–892 (1988).
5. J. Zou, S. Shivkumar and D. Apelian, Modeling of porosity formation in grain refined aluminum castings. In *Materials Processing in the Computer Age* (Edited by V. R. Voller, M. S. Stachowicz and B. G. Brian), pp. 389–401, TMS/AIME, PA (1991).
6. R. B. Bird, W. E. Stewart and E. N. Lightfoot, *Transport Phenomena*. John Wiley, New York (1960).
7. D. C. Weckman and P. Niessen, A numerical simulation of the D. C. continuous casting process including nucleate boiling heat transfer, *Metall. Trans. B*, **13B**, 593–602 (1982).
8. C. Kattel and H. Kroemer, *Thermal Physics* (2nd Edn), Chap. 3. W. H. Freeman, San Francisco, CA (1980).
9. J. Zou and M. Rappaz, Experiment and modeling of gray cast iron solidification. In *Materials Processing in the Computer Age* (Edited by V. R. Voller, M. S. Stachowicz and B. G. Brian), pp. 335–348, TMS/AIME, PA (1991).
10. H. Saito and L. E. Scriven, Studying of coating flow by the finite element method, *J. Comp. Phys.* **42**, 53–60 (1981).
11. J. M. Floryan and H. Rasmussen, Numerical methods for viscous flows with moving boundaries, *Appl. Mech. Rev.* **42**(12), 323–340 (1989).
12. P. M. Gresho, R. L. Lee and R. L. Sani, On the time dependent solution of the incompressible Navier–Stokes equations in two and three dimensions. In *Recent Advances in Numerical Methods in Fluids*. Pineridge Press, Swansea (1980).
13. W. D. Bennon, The prediction of macrosegregation in continuously cast DC ingot, Alcoa Report, Alcoa Center, PA (1989).
14. E. B. Becker, G. F. Carey and J. T. Oden, *Finite Elements, An Introduction*, Vol. 1. Prentice-Hall, Englewood Cliffs, New Jersey (1981).
15. O. C. Ziewkiewicz and C. A. Taylor, *The Finite Element Method*. McGraw-Hill, New York (1989).
16. H. Lamb, *Hydrodynamics*. Dover Press, New York (1963).
17. V. R. Voller, A. D. Brent and C. Prakash, The modeling of heat, mass and solute transport in solidification systems, *Int. J. Heat Mass Transfer* **32**(9), 1719–1731 (1989).
18. J. A. Dantzig, Modeling liquid–solid phase changes with melt convection, *Proceedings of Second FIDAP Users' Conference*, paper 6, The Fluid Dynamics International, Evanston, IL (1988).
19. A. Joly and R. Mehrabian, The rheology of a partially solid alloy, *J. Mater. Sci.* **11**, 1393–1418 (1976).
20. B. Q. Li, J. C. Liu and J. A. Brock, Numerical simulation of transient fluid flow and solidification phenomena during continuous casting of aluminum. In *Materials Processing/EPD Congress* (Edited by J. P. Hager), pp. 841–857, TMS/AIME, PA (1993).
21. T. L. Finn, W. D. Bennon and M. G. Chu, Verification of numerical predictions of macrosegregation in continuously cast ingots. In *Macro and Micro Scale Phenomena in Solidification* (Edited by C. Beckermann, J. S. Pien and R. Smelser), pp. 1–6. ASME, New York (1991).
22. B. Q. Li and Y. Ruan, An integrated finite element model for transient fluid flow and thermal stresses during continuous casting, *Int. J. Thermal Stresses*, in press.